



Chinese Society of Aeronautics and Astronautics
& Beihang University

Chinese Journal of Aeronautics

cja@buaa.edu.cn
www.sciencedirect.com



Effects of relative thickness on aerodynamic characteristics of airfoil at a low Reynolds number



Ma Dongli ^{*}, Zhao Yanping, Qiao Yuhang, Li Guanxiong

School of Aeronautic Science and Engineering, Beihang University, Beijing 100191, China

Received 21 July 2014; revised 6 November 2014; accepted 4 December 2015
Available online 21 June 2015

KEYWORDS

Aerodynamic characteristics;
Airfoil;
Laminar separation;
Low Reynolds number;
Numerical simulation;
Relative thickness;
Water tunnel model tests

Abstract This study focuses on the characteristics of low Reynolds number flow around airfoil of high-altitude unmanned aerial vehicles (HAUAVs) cruising at low speed. Numerical simulation on the flows around several representative airfoils is carried out to investigate the low Reynolds number flow. The water tunnel model tests further validate the accuracy and effectiveness of the numerical method. Then the effects of the relative thickness of airfoil on aerodynamic performance are explored, using the above numerical method, by simulating flows around airfoils of different relative thicknesses (12%, 14%, 16%, 18%), as well as different locations of the maximum relative thickness ($x/c = 22\%, 26\%, 30\%, 34\%$), at a low Reynolds number of 5×10^5 . Results show that performance of airfoils at low Reynolds number is mainly affected by the laminar separation bubble. On the premise of good stall characteristics, the value of maximum relative thickness should be as small as possible, and the location of the maximum relative thickness ought to be closer to the trailing edge to obtain fine airfoil performance. The numerical method is feasible for the simulation of low Reynolds number flow. The study can help to provide a basis for the design of low Reynolds number airfoil.

© 2015 The Authors. Production and hosting by Elsevier Ltd. on behalf of CSAA & BUAA. This is an open access article under the CC BY-NC-ND license (<http://creativecommons.org/licenses/by-nc-nd/4.0/>).

1. Introduction

High-altitude unmanned aerial vehicles (HAUAVs) develop rapidly with the gathering attention of the near space flight platform in recent years. The HAUAVs cruise in the near space and have been advanced to enable higher operational

altitudes, longer durations with greater payloads and increased autonomy. The atmosphere there has low density and high viscosity, which leads to the aerodynamics problem at low Reynolds number Re (generally less than 1 million).

As early as the 1900s, researchers found that flows behave in strange ways at Reynolds number below 1 million, compared with high Reynolds number. In low Reynolds number regime, the lift curve of symmetrical airfoil around the angle of attack of 0° acts undesirable peculiar nonlinear features. Some other airfoils produce a different type of hysteresis loop in the lift and drag forces.^{1,2} Laminar separation bubble (LSB) shown in Fig. 1, which was presented by Horton in 1968, characterizes the low Reynolds number airfoil aerodynamics.³ The bubble involves the separation of the laminar boundary layer

* Corresponding author. Tel.: +86 10 82338635.

E-mail address: madongli@buaa.edu.cn (D. Ma).

Peer review under responsibility of Editorial Committee of CJA.



Production and hosting by Elsevier

from the surface due to a strong adverse pressure gradient and the reattachment of the shear layer shortly downstream. The region between the separation and the reattachment point is called the separation bubble. Carmichael⁴ carried out the survey of low Reynolds number airfoils in 1982. He made a research on airfoil performance as well as flow separation in low Reynolds number and gave the further explanation of laminar separation bubble in detail. Mueller² presented an experimental study of the Lissaman 7769 and Miley M06-13-128 airfoils at low chord Reynolds numbers in 1985 and found that each airfoil produces a different type of hysteresis loop in the lift and drag forces when operated below chord Reynolds numbers of 300000. He claimed that it is the relative location of laminar separation and transition, which depends upon the shape of airfoil, that affects the type of hysteresis loop. Selig et al.¹ took lift and drag measurements on 34 airfoils at low Reynolds number in 1996. A plateau in the lift curve of symmetrical airfoil in the vicinity of an angle of attack 0° was found to be common in the Reynolds number range of 40000 to 100000. The nonlinearity can be reduced owing to a reduction in the size of the laminar separation bubble by the use of zig-zag type boundary-layer trip. Langley research center^{5,6} made an experimental study of the Eppler387 airfoil in the Langley Low-Turbulence Pressure Tunnel in both 1988 and 1990, focusing on the laminar separation bubble. The tests were conducted over the chord Reynolds number ranging from 60000 to 460000. Oil flow visualization was used to determine laminar separation and turbulent reattachment locations. Lots of experimental results, such as lift and pitching-moment data, were obtained. Sahin et al.⁷ carried out time-dependent unsteady calculations of low Reynolds number flows over the Eppler387 airfoil in both two- and three-dimensions, using unstructured grid associated with method of direct numerical simulation. Lift and drag coefficients calculated in each case show good agreements with extensive experimental results.

Few domestic researches focus on the low Reynolds number area. Bai et al.⁸ conducted a numerical simulation on the laminar separation of the Eppler387 airfoil near the trailing edge at low Reynolds number ranging from 60000 to 200000 and gave the conclusion that the laminar separation bubble is actually the periodical shedding of the vortex. The researches of peculiar nonlinear phenomenon of symmetrical airfoil studied by Bai⁹, Lei et al.¹⁰ described the micro vortex structure of laminar separation bubble in detail by numerical methods. Ran et al.¹¹ made numerical computations for the symmetrical airfoils at low Reynolds number ranging from 500 to 50000. The dynamic aerodynamic characteristics were studied as to different values of maximum relative thickness and position.

Computational fluid dynamics (CFD) can be used where low Reynolds number flows are too difficult to investigate experimentally.¹² Extensive previous work has proved the accuracy and effectiveness of numerical methods. The HAUAVs usually adopt the high aspect ratio design, which leads to a more crucial matter of airfoil performance. However, few researches are aiming at the airfoil of HAUAVs. In this paper, low Reynolds number flow mechanism is expounded by the numerical simulation of several airfoils using Reynolds-averaged Navier-Stokes (RANS) equations combined with transition model. In addition, water tunnel tests are carried out in order to further testify the numerical method, in the meantime, to observe the laminar

separation bubbles along with the flow regime in low Reynolds number. Finally, the numerical method is applied to calculate aerodynamic characteristics of airfoils of different relative thicknesses, to investigate the effects of relative thickness on airfoil performance. The airfoil used for HAUAVs is usually designed in big maximum relative thickness for the sake of structural strength, which would bring with the loss of aerodynamic forces. Meanwhile the laminar separation bubble would change according to the variation of thickness, which affects the airfoil performance. The study of thickness is carried out in this paper, which may help to provide a basis for the design of low Reynolds number airfoil.

2. Computation scheme

2.1. Governing equation

The governing equations are the RANS equations and the continuity equations without the gravity and the body force item in Cartesian tensor form:

$$\frac{\partial \rho}{\partial t} + \frac{\partial}{\partial x_i} (\rho u_i) = 0$$

$$\frac{\partial}{\partial t} (\rho u_i) + \frac{\partial}{\partial x_j} (\rho u_i u_j) = -\frac{\partial p}{\partial x_i} + \frac{\partial}{\partial x_j} \left(\mu \frac{\partial u_i}{\partial x_j} - \rho \bar{u}_i \bar{u}_j \right) + S_i \quad (1)$$

where ρ is the density, u_i the velocity component of i direction, p the pressure, μ the dynamic viscosity of the fluid, $-\rho \bar{u}_i \bar{u}_j$ the Reynolds stress, and S_i the generalized source term.

2.2. Transition model

Transition prediction is a difficult and key topic in low Reynolds number flows. Transition empirical formula, hydrodynamic stability theory and transition prediction formulation of the e^N type are three main transition prediction methods. Langtry and Menter proposed transition shear stress transport (SST) model, which is combined with the SST $k - \omega$ the calculation model, readers can refer to Ref model and the $\gamma - \tilde{R}_{\theta}$ model at 2005.¹³ The model is based on the coupling of the SST $k - \omega$ transport equations with two other transport equations, one for the intermittency and one for the transition onset criteria, in terms of momentum-thickness Reynolds number. The transport equation for the intermittency, γ , reads:

$$\frac{\partial(\rho\gamma)}{\partial t} + \frac{\partial(\rho U_j \gamma)}{\partial x_j} = P_{\gamma 1} - E_{\gamma 1} + P_{\gamma 2} - E_{\gamma 2} + \frac{\partial}{\partial x_j} \left[\left(\mu + \frac{\mu_t}{\sigma_{\gamma}} \right) \frac{\partial \gamma}{\partial x_j} \right] \quad (2)$$

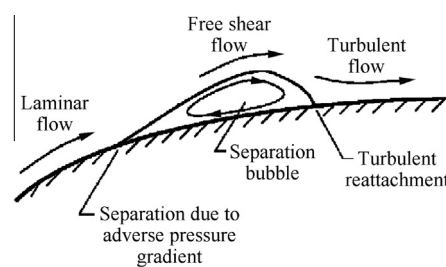


Fig. 1 Laminar separation bubble.³

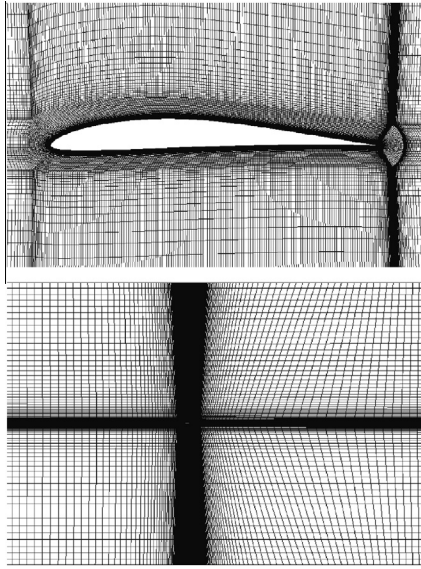


Fig. 2 Computational grid and Eppler387 airfoil geometry.

where $P_{\gamma 1}$ and $E_{\gamma 1}$ are transition sources, $P_{\gamma 2}$ and $E_{\gamma 2}$ are the destruction sources and relaminarization sources respectively. Due to the laminar separation bubbles at low Reynolds number, the modification of intermittency γ for separation-induced transition is shown as

$$\gamma_{\text{sep}} = \min \left(2 \max \left(\frac{Re_v}{3.235 Re_{\theta c}} - 1, 0 \right) \exp \left(- \left(\frac{R_t}{20} \right)^4 \right), 2 \right) F_{\theta t} \quad (3)$$

Finally, the effective intermittency γ is calculated as:

$$\gamma_{\text{eff}} = \max(\gamma, \gamma_{\text{sep}}) \quad (4)$$

The transport equation for the transition momentum thickness Reynolds number, $\tilde{Re}_{\theta t}$, reads:

$$\frac{\partial(\rho \tilde{Re}_{\theta t})}{\partial t} + \frac{\partial(\rho U_j \tilde{Re}_{\theta t})}{\partial x_j} = P_{\theta t} + \frac{\partial}{\partial x_j} \left[\sigma_{\theta t} (\mu + \mu_t) \frac{\partial \tilde{Re}_{\theta t}}{\partial x_j} \right] \quad (5)$$

where $P_{\theta t}$ is the source term.

Then, the transition model interacts with the SST $k - \omega$, as follows:

$$\begin{cases} \frac{\partial}{\partial t} (\rho k) + \frac{\partial}{\partial x_j} (\rho u_j k) = \tilde{P}_k - \tilde{D}_k + \frac{\partial}{\partial x_j} \left((\mu + \sigma_k \mu_t) \frac{\partial k}{\partial x_j} \right) \\ \tilde{P}_k = \gamma_{\text{eff}} P_k \\ \tilde{D}_k = \min(\max(\gamma_{\text{eff}}, 0.1), 1.0) D_k \end{cases} \quad (6)$$

where P_k and D_k are the original production and destruction terms for the SST model. For detailed information about the calculation model, readers can refer to Ref. ¹³.

2.3. Grid generation

Numerical simulation needs fine computational grid in low Reynolds number flows. The structured grid is more preferable than unstructured grid since it can avoid the divergence caused by rough grid. The H-type mesh generated by elliptical method

is more suitable for the flow simulation at low Reynolds number.¹⁴ The computational grid, shown in Fig. 2, constitutes 200 grid points on the airfoil surface. The chord length is c , and the respective distance of the front and back boundaries away from the leading edge and the trailing edge is $15c$ and $20c$. The up and down boundaries is $15c$ away from the chord. In order to capture the laminar and transitional boundary layers correctly, the grid must have a y^+ of approximate to one.¹³ y^+ is a non-dimensional distance which indicates the degree of fineness of grid in near-wall region. It is defined by the formula:¹⁵

$$y^+ = \frac{\sqrt{\tau_w / \rho \Delta y}}{v} \quad (7)$$

where τ_w is the wall shear stress, Δy the gap between the wall and the first layer of grid, and v the kinetic viscosity coefficient, respectively.

3. Numerical method validation

3.1. Validation of lift and drag forces of Eppler387 airfoil

Eppler387 airfoil is one of the representative airfoils of high altitude propeller and HAUAVs. Extensive experimental studies of it have been conducted in order to determine the performance characteristics of airfoils at low Reynolds numbers.^{5,6} Fig. 2 shows the shape of airfoil and the computational grid. Computational grid has a y^+ of approximate to one and contains 70000 grids. Governing equations have a precision of second-order, and pressure–velocity coupling adopts the Semi-implicit method for pressure-linked equations-consistent (SIMPLEC) algorithm. Fig. 3 shows the results of lift coefficient C_L and drag coefficient C_D at a Reynolds number of 300000, α is the angle of attack. The computation results meet well with the experimental measurements, which proves the credibility of the numerical method.

3.2. Validation of nonlinear lift curve of SD8020 airfoil

Research shows that the peculiar nonlinear features of the lift curve of symmetrical airfoil around angle of attack of 0° attribute to the laminar separation bubbles.¹ Fig. 4 shows the comparison of computation results and experimental measurements of SD8020 airfoil at Re of 40000 and 100000. Computation results are consistent with the experimental data. As seen, the lift characteristics are not typical of those found for higher Reynolds number airfoil flows in which the lift curve is nearly with a slope of 2π . At a Re of 40000, in the vicinity of 0° , the slope is less than 2π , therefore, a plateau occurs. The phenomenon is not apparent at a Re of 100000, which indicates that it is sensitive to Reynolds number. With the increase of Reynolds number, the nonlinear features alleviate and disappear.

The time-averaged streamlines of SD8020 airfoil at a Re of 40000 are shown in Fig. 5. As the angle of attack is increased, the pressure gradient on the upper surface steepens, and the upper surface bubble grows larger and moves upstream, while the lower surface bubble acts in the opposite way. It shrinks in size and moves downstream. The bubble increases the displacement thickness, which effectively changes the camber. At the negative angle of attack, the existence of bubble results in

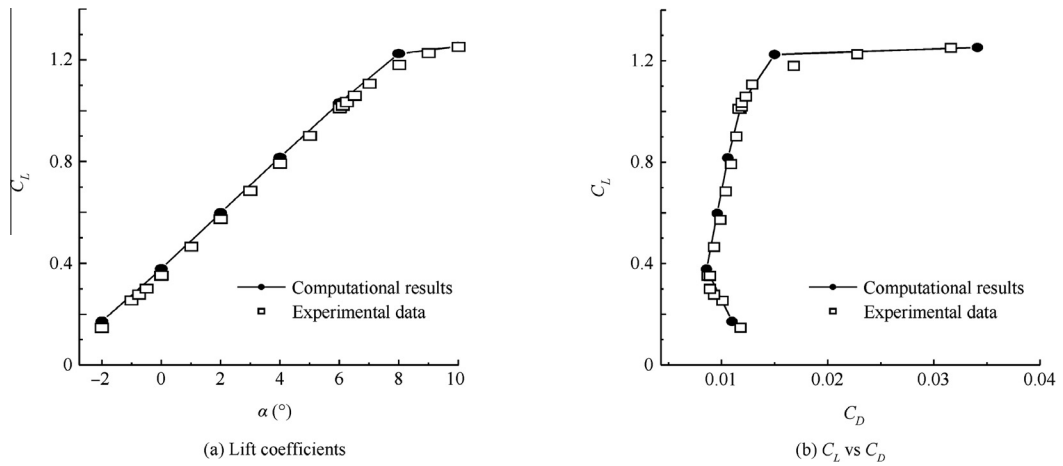


Fig. 3 Comparison of aerodynamic characteristics for an Eppler387 airfoil at $Re = 300000$.

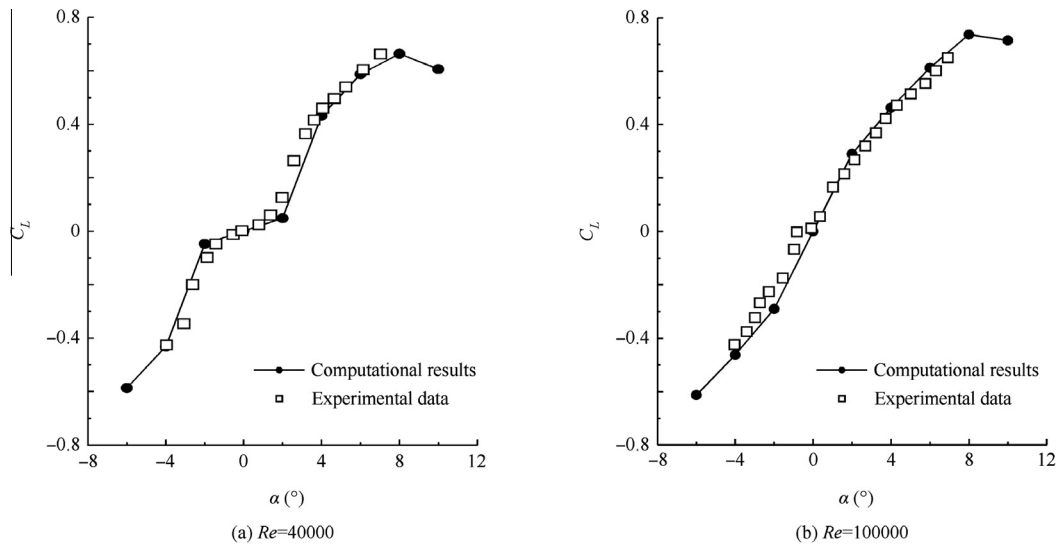


Fig. 4 Comparison of aerodynamic characteristics for an SD8020 airfoil.

positive camber which decreases as the angle increases. Consequently, the lift is reduced relative to what might be expected when laminar separation bubble effects are ignored. At the positive angle of attack, the bubble leads to a negative camber, which results in the reduced of lift. After angle of attack of 2° , the laminar separation bubble moves upstream and is away from the trailing edge, which effectively causes the positive camber. Therefore, the lift increases rapidly. The behavior of laminar separation bubble accounts for the initial deadband in the vicinity of angle of attack of 0° , which affects the performance of symmetrical airfoil. Numerical calculation can reveal the phenomenon.

4. Water tunnel tests

In order to further verify the numerical method and to observe the laminar separation bubbles as well as the flow regime in

low Reynolds number visually, water tunnel tests are applied to testing two airfoils. Airfoil I has a maximum relative thickness of 15%, while Airfoil II is about 13%. The experiments are performed in the 1.2 m multi-purpose low-speed water tunnel at Beihang University. The schematic of tunnel is shown in Fig. 6. The tunnel, with a whole length of 85 m, is considered as the largest low-speed water tunnel in Asia. The main test section is nominally $1.2 \text{ m} \times 1.0 \text{ m}$ in cross-section and 2.1 m long. The water speed ranges from 0.1 to 1.0 m/s, with a flow uniformity of 0.46%, and the turbulence intensity is within the scope of 0.27%–0.45%.

The airfoil model is set within the test section horizontally, as shown in Fig. 7. Glass end plates are added on both sides of the model to avoid the stream being up and down. Staining solution and hydrogen bubble visualization are used to visualize the flow. Each of the model is made of aluminum alloy, with a chord of 1.7 m and a span of 0.9 m. As shown in

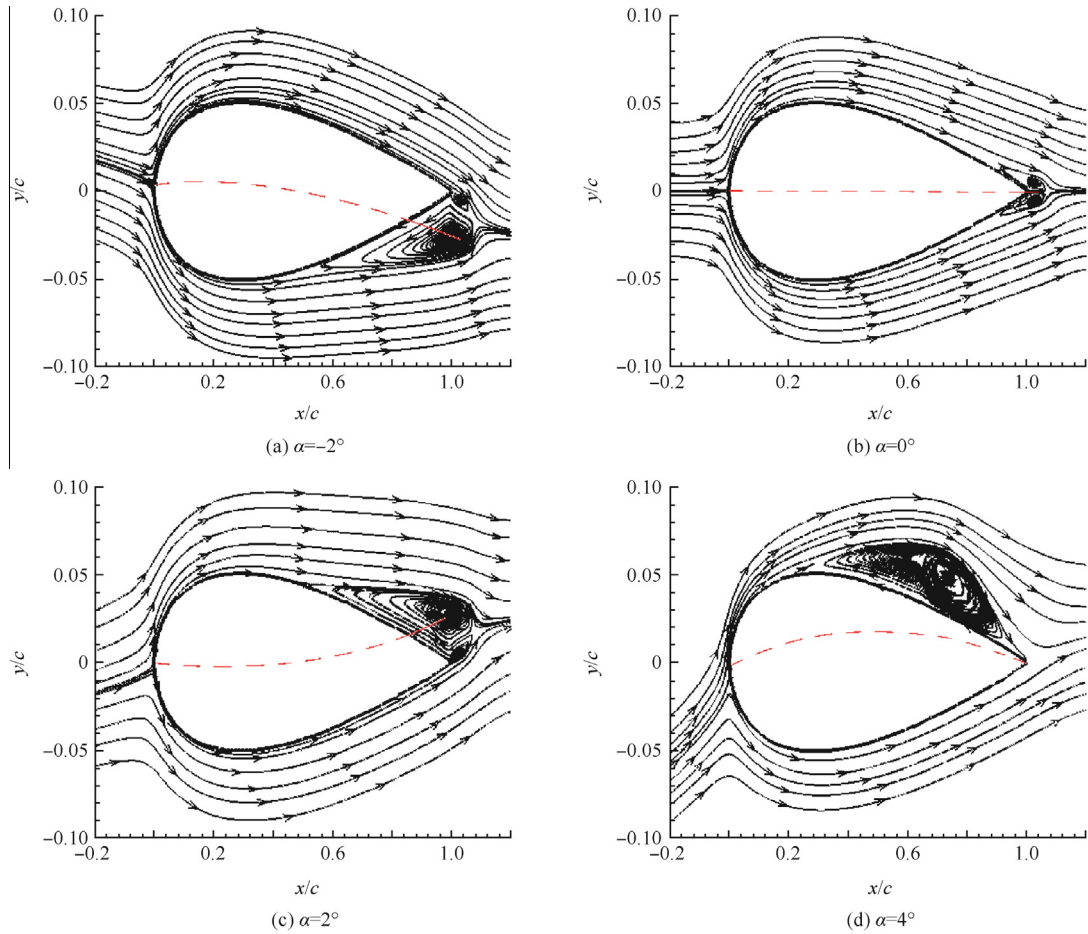


Fig. 5 Time-averaged streamlines of SD8020 airfoil at $Re = 40,000$.

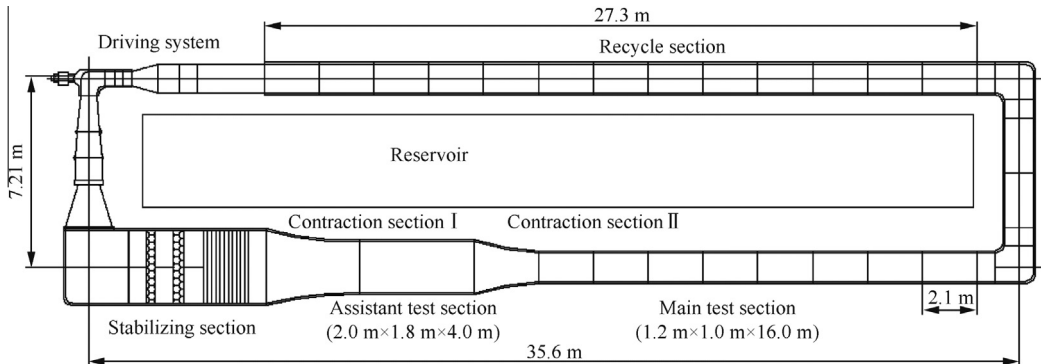


Fig. 6 Schematic of low-speed water tunnel at Beihang University.

Fig. 8(a), holes used for injecting staining solution are punched every 5% chord length on both the upper and lower surfaces. **Fig. 8(b)** displays the staining solution supply system. There are two kinds of staining solution of different colors. The red one is injected in the chord location of 10%, 20%, 30%, etc., while the blue one is for the location of 5%, 15%, 25%, et al. Lots of air bubbles are found to stick to the lower surface, which disturbs the flow regime. In addition, lower-surface laminar flow is seen to exist from the leading edge to

the trailing edge under most of the test conditions, which cannot show the whole process of separation, transition and reattachment of the flow. Hence, analyses are merely conducted on the test results of upper surface. Observation of flow over airfoils at three water speeds (0.2, 0.3, 0.4 m/s), corresponding to three Reynolds numbers (323000, 484000, 645000), has been carried out. The test Reynolds numbers are slightly different from that of numerical simulation, but are in the same order of magnitude.

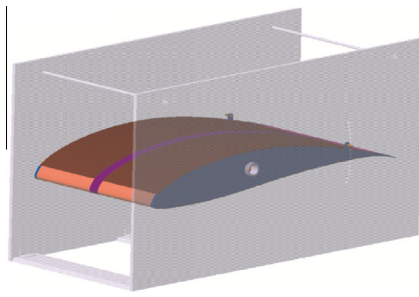


Fig. 7 Airfoil model layout.

4.1. Staining solution visualization

Fig. 9(a) shows the upper surface of Airfoil I at 4° angle of attack at a speed of 0.2 m/s ($Re = 323000$). Staining solution grows darker at the chord location of 35.5% , which indicates the separations occur. The upstream is stable and maintains the laminar flow. The transition begins at the location of about 47.0% where the liquid becomes disorderly. **Fig. 9(b)** illustrates the laminar separation bubble in detail. The color liquid accumulation indicates the existence of separation. Transition takes place in the free shear layer above the surface. Downstream of this point, reattachment occurs in a process that is known to be unsteady as vortices are periodically generated and impinge on the surface. What between the separation point and the reattachment forms the laminar separation bubble. **Fig. 9(c)** is the time-averaged streamlines and turbulent kinetic energy contour of the simulation results

of upper-surface flow around Airfoil I under the corresponding condition. The red color region of contour means high turbulent kinetic energy, which infers transition of flow. As seen, the size and location of bubble along with the transition show good agreement with what is observed in the experiment. **Fig. 9(d)** illustrates the connection between the laminar separation bubble and the skin friction coefficient C_f distribution. Laminar flow is seen to exist from the leading edge to approximately $x/c = 30\%$ because of the positive sign of C_f .¹⁶ Then separation begins at the point where $C_f = 0$ and ends where C_f turns from negative to positive at $x/c = 50\%$. The flow is mainly stagnant in this region and is consistent with the so-called laminar separation bubble. As sketched, the magnitude of the C_f in this region is quite small because of the low flow speed and negative in sign because of reverse flow on the surface. The beginning of separation cannot be detected obviously in experiment since it is not distinct, and the reattachment line is less evident on account of the instability of turbulent flow. Hence, the records of test are slightly different from what is illustrated by C_f curve, which is acceptable.

Fig. 10(a) shows the upper surface of Airfoil II at the same condition compared to Airfoil I. Separation takes place at approximately $x/c = 47.5\%$ and transition is at 60.0% . **Fig. 10(b)** illustrates the laminar separation bubble in detail. The whole process of separation, transition and reattachment can be seen clearly. The corresponding simulation results of time-averaged streamlines, as well as the turbulent kinetic energy contour, shown in **Fig. 10(c)**, are consistent with what is observed in the experiment. **Fig. 10(d)** is the C_f curve of upper surface. The separation exists from the chord location of 50% till around 68% . Downstream of reattachment, the boundary layer is, of course, turbulent, until approximately $x/c = 98\%$. C_f turns negative in sign again and indicates the existence of slight turbulent separation.

4.2. Hydrogen bubble visualization

Hydrogen bubble visualization adopts to the upper-surface flow of Airfoil II at a water speed of 0.2 m/s . Water can be reduced to oxygen and hydrogen by electrolysis. The hydrogen bubbles are generated from the negative pole which is made of platinum wire of $20 \mu\text{m}$ in diameter. The generating bubble is $10 \mu\text{m}$ in diameter and is not easy to float up and follows the flow well. The Reynolds number based on the diameter of platinum wire is so low that there exists no separation around the wire. Hence the interference of wire can be ignored. Impulse generator takes control of the hydrogen bubbles. The frequency is 10 Hz , along with a duty ratio of 50% , and the voltage is 10 V . **Fig. 11** shows the flow of upper surface at angle of attack of 4° . The platinum wire is located at $x/c = 40.0\%$. As seen, the timelines are distinct and bubble stripes are in order until approximately $x/c = 47.5\%$, which indicates that the laminar flow exists upstream. Downstream of that point, the timelines become vague and the hydrogen bubbles gather, which means the laminar separation bubble occurs. About $x/c = 60.0\%$, where the hydrogen bubbles are in chaos, transition begins.

Fig. 12 illustrates the turbulent kinetic energy k curve of upper surface under the same condition. Laminar flow exists from the leading edge to the approximately $x/c = 60.0\%$ since the turbulent kinetic energy value is quite small. A surge in

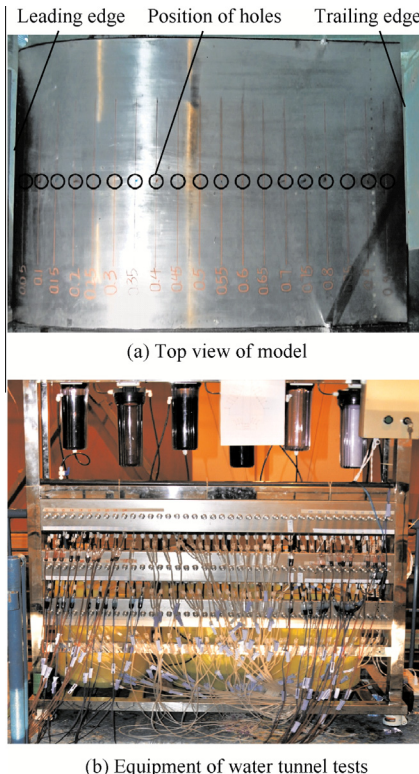


Fig. 8 Model and equipment of water tunnel tests.

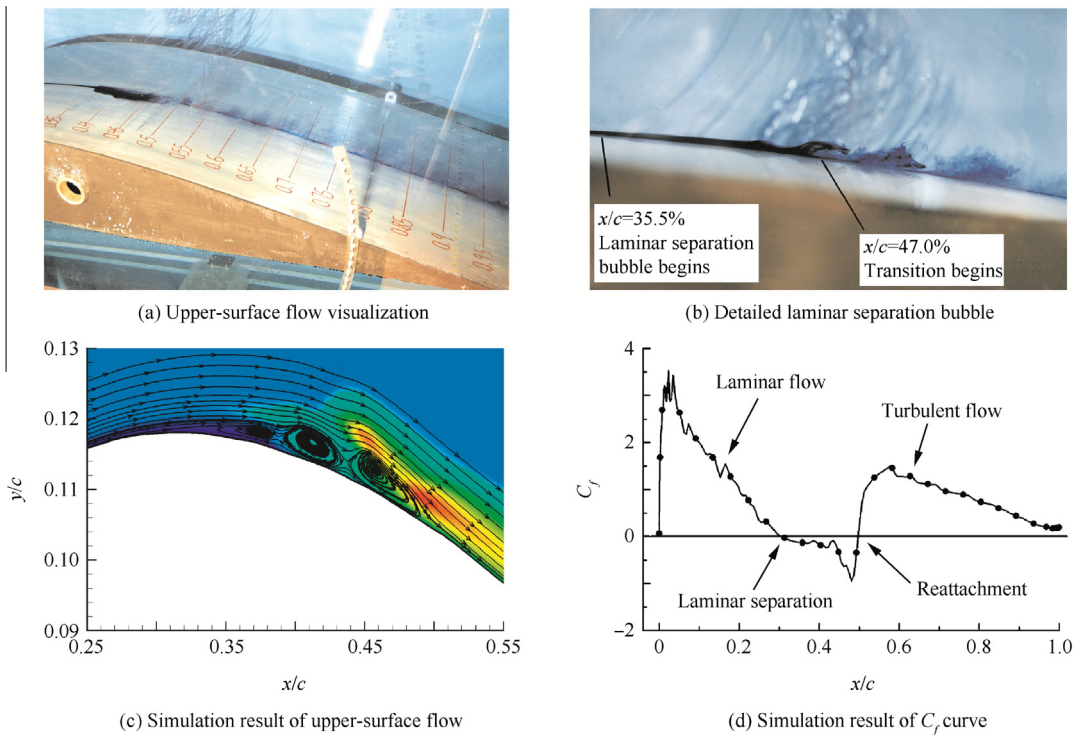


Fig. 9 Upper-surface flow characteristics of Airfoil I at $\alpha = 4^\circ$, $Re = 323000$.

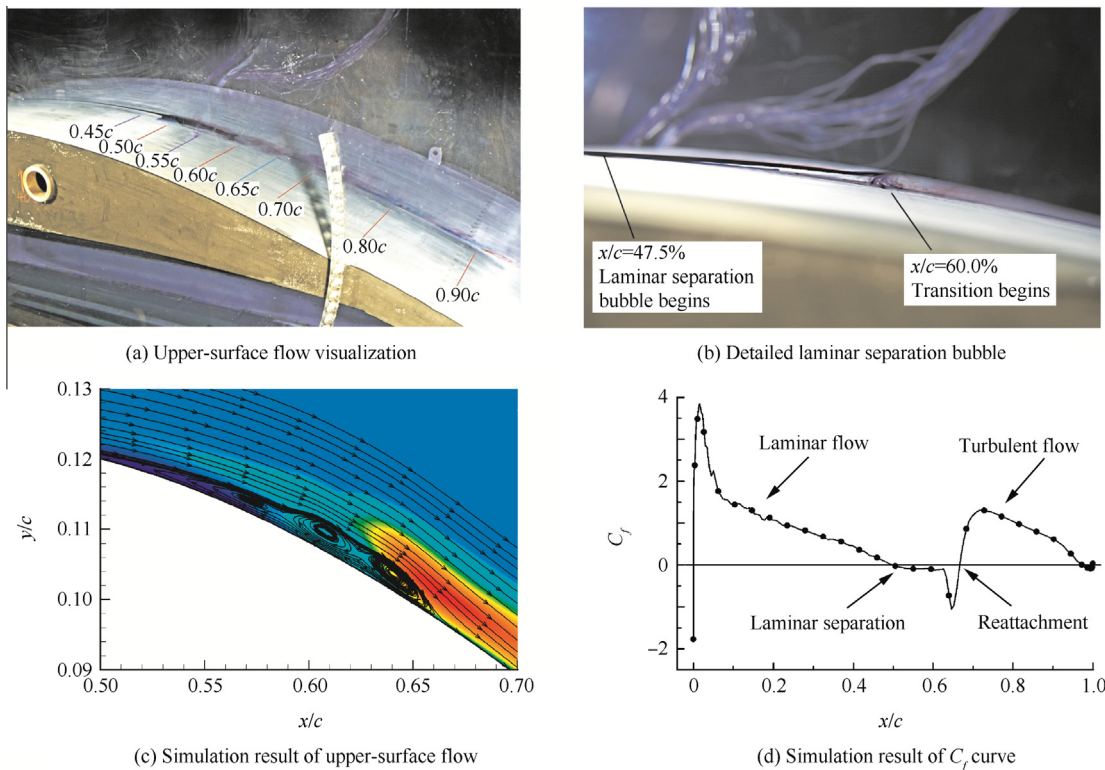


Fig. 10 Upper-surface flow characteristics of Airfoil II at $\alpha = 4^\circ$, $Re = 323000$.

turbulent kinetic energy signifies that transition happens. Then it maintains at a high level and is weakened owing to the inverse pressure gradient till the trailing edge.

The observation results are recorded in [Table 1](#). All data come from the upper surface of airfoils. There are no records about the location of reattachment because it is closed to the

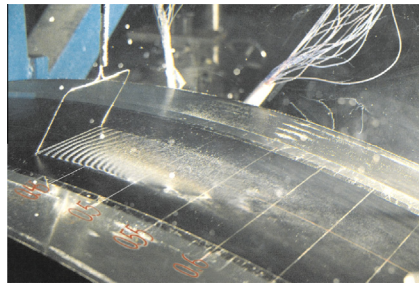


Fig. 11 Flow visualization by hydrogen bubbles of Airfoil II at $\alpha = 4^\circ$, $Re = 323000$.

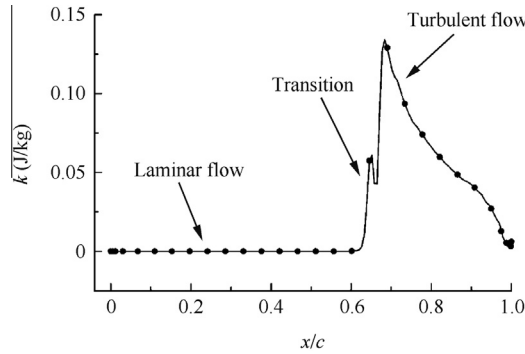


Fig. 12 Turbulent kinetic energy curve of Airfoil II at $\alpha = 4^\circ$, $Re = 323000$.

Table 2 Main parameters of airfoils (Case 1).

Airfoil	Camber	x_t/c (%)	t/c (%)
a	Maximum camber is 6.09% at $x/c = 55\%$	30	12
b			14
c			16
d			18

Notes: x_t/c is the location of maximum relative thickness, t/c is the maximum relative thickness value.

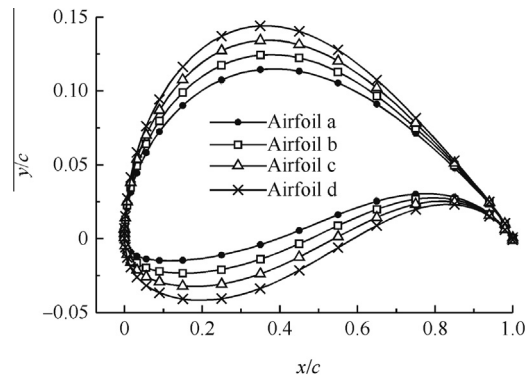


Fig. 13 Shape of airfoils of different relative thickness values.

Table 1 Comparison of laminar separation bubble along with transition for upper-surface flow around airfoils.

Airfoil	Reynolds number	α ($^\circ$)	Computation result of start location (%)		Experimental data of start location (%)		Absolute error (%)	
			LSB	Transition	LSB	Transition	LSB	Transition
I	323000	-4	50	70	54	68	-4	2
		-2	48	62	50	62.5	-2	-0.5
		0	42	58	45	56.5	-3	1.5
		2	36	52	40	52	-4	0
		4	30	48	35.5	47	-5.5	1
		6	26	44	32	42	-6	2
	645000	-4	54	66	57	63	-3	3
		-2	48	60	51	57	-3	3
		0	44	54	47	52.5	-3	1.5
		2	36	48	39	46	-3	2
II	323000	4	30	42	38	41	-8	1
		6	26	36	32.5	36.5	-6.5	-0.5
		-4	60	80	63.5	75	-3.5	5
		-2	58	72	58	71.5	0	0.5
		0	56	70	54.5	67	1.5	3
	484000	2	52	68	51	64	1	4
		4	50	60	47.5	60	2.5	0
		6	44	60	43	55	1	5
		-4	62	76	63.5	74	-1.5	2
		-2	60	72	59	69	1	3
III	645000	0	56	68	56	65	0	3
		2	56	64	52.5	62	3.5	2
		4	50	60	49	56.5	1	3.5
		6	44	56	44	52.5	0	3.5
		-4	62	72	64.5	72	-2.5	0
	484000	-2	60	72	60	67	0	5
		0	56	68	56	63	0	5
		2	56	64	53	60	3	4
		4	50	60	50	55	0	5
		6	48	56	43	50	5	6

position where transition occurs and is not distinct. Known from the analysis of error, the calculated results show good agreement with the experimental data at a small angle of attack. The maximum absolute error of Airfoil II is less than 6% chord length. The error grows roughly with the increase of angle of attack or of the water speed. The reason may be that the tiny air bubbles sticking to the upper surface disturb the flow, and the disorder following transition interferes with the records. In addition, compared with Airfoil I, the laminar separation begins later in Airfoil II, hence, the laminar flow can exist longer. The maximum relative thickness of Airfoil II is different from that of Airfoil I, which infers that the relative thickness has an effect on the flow regime over an airfoil

and affects aerodynamic characteristics. The water tunnel tests display the flow performance visually and verify the accuracy and effectiveness of numerical method once more.

5. Analysis of effects of airfoil relative thickness

Research on the effects of relative thickness on airfoil aerodynamic characteristics at a low Reynolds number of 500000 is carried out using the numerical method. The basic airfoil is a modification of fx63-137 airfoil. It has a maximum relative thickness of 14% at the $x/c = 30\%$. The camber is 6.09% at the $x/c = 55\%$. Compared with symmetrical airfoils, it is

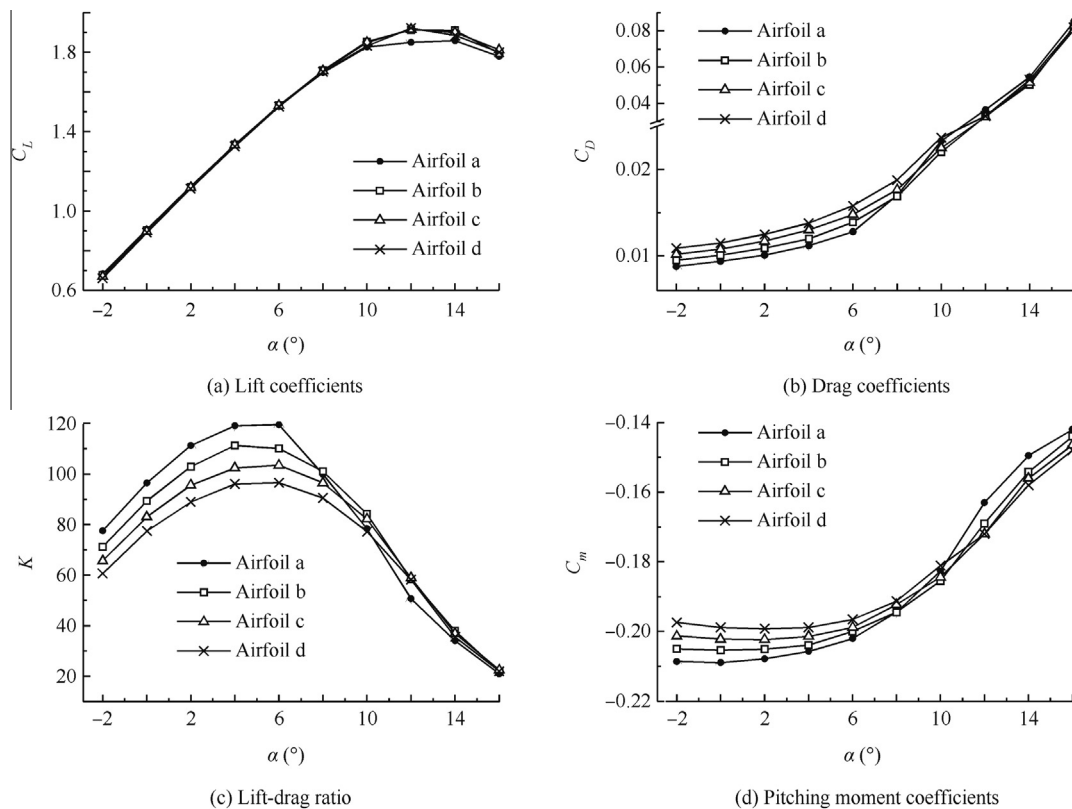


Fig. 14 Aerodynamic characteristics of airfoils with different relative thickness values.

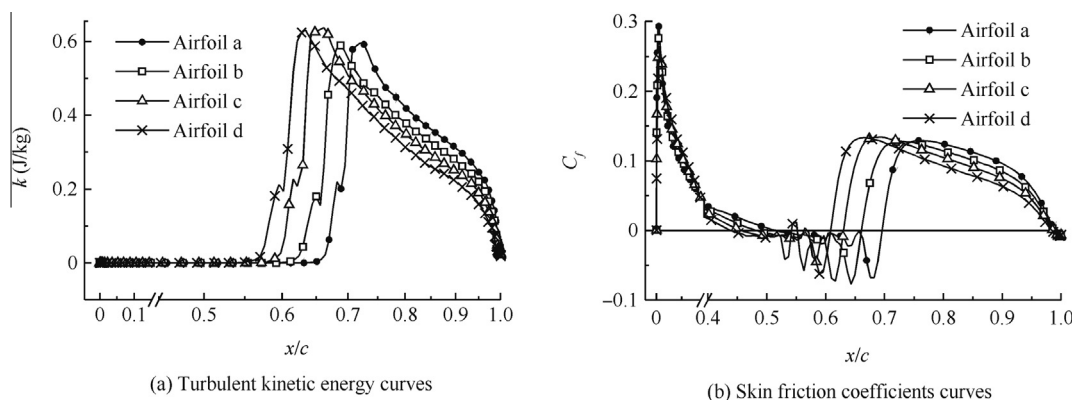


Fig. 15 Turbulent kinetic energy and skin friction coefficients curves of upper-surface flow at $\alpha = 2^\circ$, $Re = 500000$.

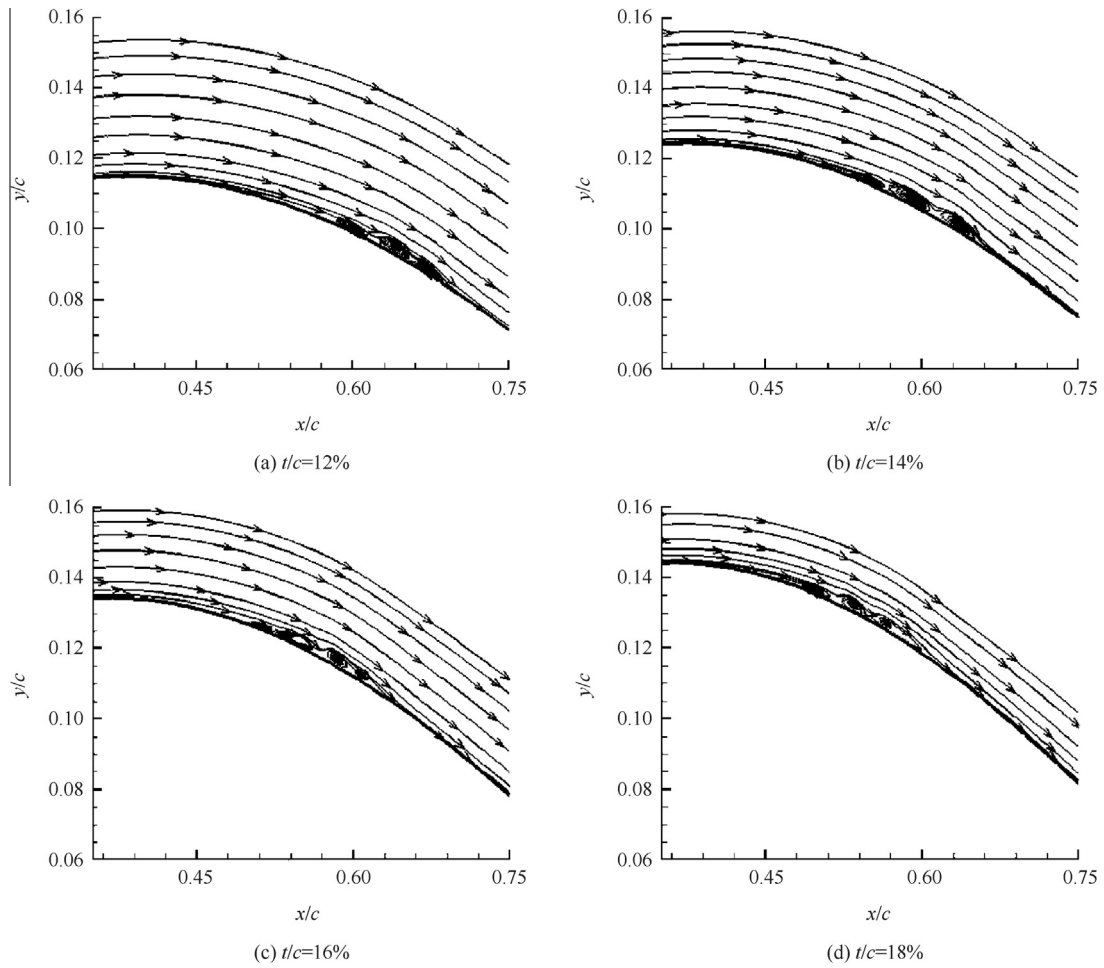


Fig. 16 Laminar separation bubbles of upper-surface flow at $\alpha = 2^\circ$, $Re = 500000$.

Table 3 Main parameters of airfoils (Case 2).

Airfoil	Camber	x_t/c (%)	t/c (%)
e	Maximum camber is 6.09% at $x/c = 55\%$	22	14
f		26	
g		30	
h		34	

widely used in low Reynolds number area. Guaranteeing that the camber remains the same, the maximum of relative thickness value and its location have been changed respectively to reveal the influence that the relative thickness has on the performance of airfoil in low Reynolds number.

5.1. Effects of the maximum relative thickness value

Based on the basic airfoil, three other airfoils of different maximum relative thickness values, but of the same camber and the relative thickness location are produced. Table 2 shows the detailed information of each airfoil, along with the airfoils shape shown in Fig. 14.

Curves of aerodynamic characteristics of airfoils described in Table 2 are shown in Fig. 14, where K is lift-drag ratio,

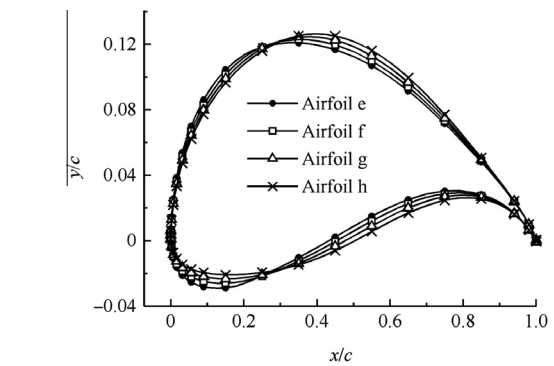


Fig. 17 Shape of airfoils at different locations with maximum relative thickness.

C_m is pitching moment coefficients. For the lift curves, the maximum thickness value has no obvious effects on the lift data at tiny angles of attack. The thicker the airfoil is, the higher the maximum lift can reach, and the more sluggishly the stall happens, but the differences are not distinct. For the drag curves, the drag data grow with the increasing thickness of airfoil at small angles of attack, and intersect when the angle

of attack is larger. For the lift-drag ratio curves, increasing the thickness leads to proportional declines of the maximum lift-drag ratio. The angle of attack, existing in the range of 4°–6°, where the maximum lift-drag ratio occurs, has nothing to do with the thickness of airfoils, generally. At large angles of attack, lift-drag ratios of thinner airfoils descend sharply while the thicker change gradually, which illustrates that the thicker airfoils perform better than the thinner at large angles of attack. In addition, for the moment curves, the larger the thickness is, the smaller the pitching moment modulus operates at tiny angles of attack, while it goes the opposite when the angle of attack grows larger. The curves cross and are generally consistent with the drag data.

The aerodynamic characteristics of airfoils have a relationship with the laminar separation bubble at low Reynolds number. Fig. 15 shows the upper-surface turbulent kinetic energy curves as well as C_f curves of airfoils at angle of attack of 2°. The surge in curve of the turbulent kinetic energy implies the transition. The sign of C_f changes in negative indicates separation. As seen, when the airfoil becomes thicker, the location of transition moves upstream, along with the laminar separation bubble. Consequently, the range of laminar flow shrinks and the drag increases. On the contrary, the location of transition moves downstream with the increase of thickness at large angles of attack, thus the range of laminar flow enlarges and the drag declines. Fig. 16 illustrates the time-averaged streamlines of upper-surface ranging from 35% to 75% chord. The laminar separation bubble moves upstream with the increase of thickness and shrinks slightly in size. Generally, on the

premise of good stall characteristics, the relative thickness value should be smaller to guarantee wide laminar flow and high lift-drag ratio at cruise.

5.2. Effects of the maximum relative thickness location

Based on the basic airfoil, three other airfoils of different locations of the maximum relative thickness, but of the same camber and the relative thickness value are produced. Table 3 shows the detailed information of each airfoil, along with the airfoils shape shown in Fig. 17.

Curves of aerodynamic characteristics of airfoils described in Table 3 are shown in Fig. 18. For the lift curves, the maximum thickness location has no obvious effects on the lift data at tiny angles of attack. The closer to the trailing edge, the location of maximum relative thickness is, the lower the maximum lift can reach, and the less sluggishly the stall happens. Starting from the angle of attack of 4°, the slope of airfoils which have a maximum thickness near the leading edge reduce slightly. For the drag curves, the drag data descend as the location of maximum thickness moves downstream, with the angle of attack from 2° to 8°. However, the trend changes to the opposite falling outside that range. In addition, the drag data of airfoils which have a location of maximum thickness near the trailing edge, though are bigger in the tiny angles of attack, grow more slowly. For the lift-drag ratio curves, as the location of maximum thickness moves downstream, the maximum lift-drag ratio becomes larger, along with the corresponding angle of attack. Meanwhile, the stall characteristics of airfoil

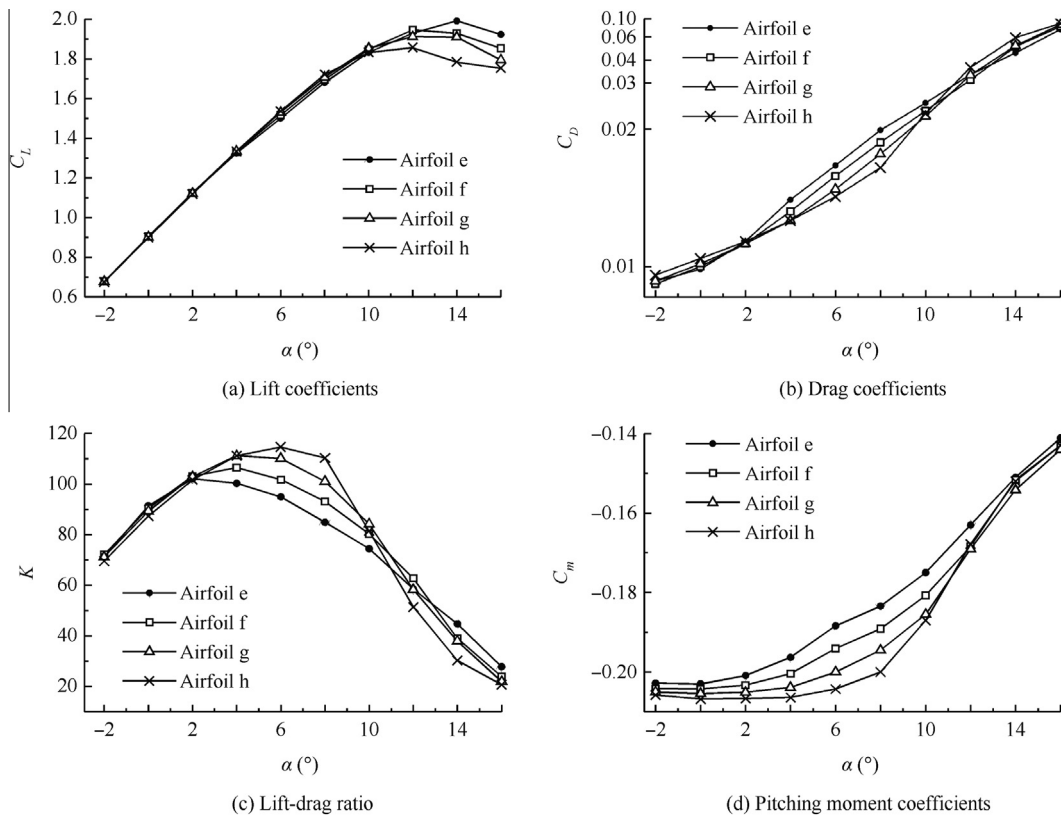


Fig. 18 Aerodynamic characteristics of airfoils at different locations with maximum relative thickness.

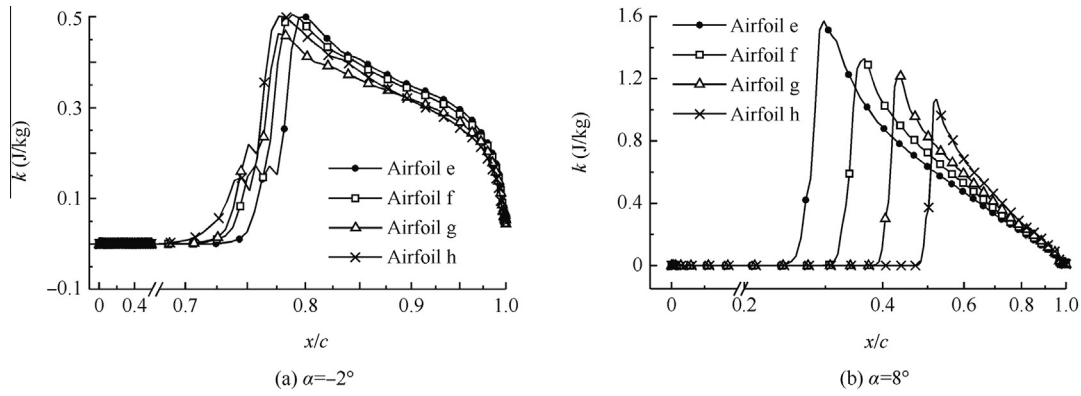


Fig. 19 Turbulent kinetic energy curves of upper-surface flow at $\alpha = -2^\circ$ and 8° , $Re = 500000$.

turn worse for the sharp falling of data at big angles of attack. The life-drag ratio is consistent with the drag data and changes at the angles of attack of 2° and 10° . Then again, for the moment curves, moving the location of maximum thickness to the trailing edge leads to the bigger moment modulus in tiny angles of attack. While at the angle of attack of 12° , the trend operates the opposite. Generally, airfoils having a location of maximum thickness closer to the trailing edge result in bigger drag forces at tiny angles of attack and worse stall characteristics, nevertheless, they act well during a wide scope of angle from -2° to 8° , and have higher lift-drag ratios. This kind of airfoil is approximate to the laminar airfoil profile. The laminar flow maintains more easily at low Reynolds number. Hence this kind of airfoil can extend the range of laminar flow to reduce drag forces.

Fig. 19 shows the turbulent kinetic energy curves of airfoils at $\alpha = -2^\circ$ and $\alpha = 8^\circ$. As seen, transition of airfoil which has a location of the maximum thickness at $x/c = 34\%$ moves upstream by 20% chord length with the angle of attack from -2° to 8° , while that of the airfoil whose location of maximum thickness is 22% moves by 48%. Therefore, the airfoil whose location of maximum thickness closer to trailing edge has smaller drag force in this region and has little effects on transition. The rank of transition curves from $\alpha = 2^\circ$ to 8° display the same as 8° angle of attack, and are the opposite of that outside. Just as the case of angle of attack being -2° , the transition trend of larger angles of attack is similar to what happens at negative angle of attack, which accounts for the crossing of drag curves. The location of laminar separation bubble is associated with the transition so the change of that is of no need to take a tautology. It is the shift of laminar separation bubble that affects the location of transition, and thus the flow regime and airfoil performance. Thus, the balance of drag, lift-drag ratio and stall characteristics ought to be taken into consideration when designing the location of maximum relative thickness of airfoil. The best location is between $x/c = 30\%$ and 34% at the Reynolds number of 500000. Both high lift-drag ratio and good stall characteristics can be achieved.

6. Conclusions

This study focuses on the characteristics of low Reynolds number flow around airfoil of HAUAVs cruising at low speed.

- (1) The low Reynolds number flow is unsteady and is not easy to be researched in quantitative experiment. Numerical simulation can calculate the aerodynamic characteristics with an acceptable accuracy. The data obtained in water tunnel tests are consistent with those of the numerical results, which verifies the validity of the numerical method.
- (2) The relative thickness affects the airfoil performance by changing the location and size of laminar separation bubble as well as the transition. Therefore, a control to laminar separation bubble can results in an improvement of aerodynamic characteristics of airfoil in low Reynolds numbers.
- (3) The increase of the maximum relative thickness value leads to the fact that the higher the maximum lift, the bigger the drag forces, the smaller the pitching-moment modulus, the lower the maximum lift-drag ratio, as well as the more sluggish stall characteristics at tiny angles of attack. The angle of attack, where maximum lift-drag ratio exists, has little to do with the relative thickness value. In addition, the relative thickness value affects the location and size of laminar separation bubble as well as transition. At small angles of attack, the larger the maximum relative thickness value is, the closer to leading edge the location of laminar separation bubble and transition is, and the smaller the bubble becomes. Thus, to obtain a higher maximum lift-drag ratio, the airfoil ought to be thinner, on the premise of good stall characteristics.
- (4) Moving closer to the trailing edge of the maximum relative thickness location results in the smaller maximum lift, the bigger drag forces, the larger pitching-moment modulus at tiny angles of attack, as well as the sharp stall characteristics, and the bigger maximum lift-drag ratio along with the corresponding angle of attack. Meanwhile, in a wide scope of angle of attack, drag forces grow slowly as the maximum relative thickness location moves downstream. Thus, the balance of drag, lift-drag ratio and stall characteristics ought to be taken into consideration when designing the location of maximum relative thickness of airfoil. The best location is between $x/c = 30\%$ and 34% at the Reynolds number of 500000. Both high lift-drag ratio and good stall characteristics can be achieved.

Relative thickness mainly affects the laminar separation bubbles and transition, so as to make an effect on the aerodynamic characteristics of airfoil. The Reynolds number of 500000, at which lots of HAUAVs cruise, is a representative of low Reynolds numbers. Hence it is meaningful to research on this Reynolds number. This study can help to provide a basis for the design of low Reynolds number airfoil.

References

1. Selig MS, Guglielmo JJ, Broern AP, Giguere P. Experiments on airfoils at low Reynolds numbers. Reston: AIAA; 1996. Report No.: AIAA-1996-0062.
2. Mueller TJ. The influence of laminar separation and transition on low Reynolds number hysteresis. *J Aircraft* 1985;22(9):763–70.
3. Horton HP. Laminar separation bubbles in two and three dimensional incompressible flow [dissertation]. London: University of London; 1968.
4. Carmichael BH. Low Reynolds number airfoil survey, volume I. Washington, D.C.: NASA Langley Research Center; 1982. Report No.: NASA-CR-165803-Vol-1.
5. McGhee RJ, Walker BS, Millard BF. Experiment results for the Eppler387 airfoil at low Reynolds in the langley turbulence pressure tunnel. Washington, D.C.: NASA Langley Research Center; 1988. Report No.: NASA-TM-4062.
6. Cole GM, Mueller TJ. Experimental measurements of the laminar separation bubble on an eppler387 airfoil at low Reynolds numbers. Washington, D.C.: NASA Langley Research Center; 1990. Report No.: UNDAS-1419-FR.
7. Sahin M, Hall J, Mohseni K. Direct numerical simulation of separated low-Reynolds number flows around an Eppler387 airfoil. Reston: AIAA; 2008. Report No.: AIAA-2008-0422.
8. Bai P, Cui EJ, Zhou WJ. Numerical simulation of laminar separation bubble over 2D airfoil at low Reynolds number. *Acta Aerodynamica Sin* 2006;24(4):416–24 Chinese.
9. Bai P, Cui EJ, Li F, Zhou WJ. Study of the nonlinear lift coefficient of the symmetrical airfoil at low Reynolds number near the 0°angle of attack. *Chin J Theor Appl Mech* 2006;38(1):1–8 Chinese.
10. Lei JM, Guo F, Huang C. Numerical study of separation on the trailing edge of a symmetrical airfoil at a low Reynolds number. *Chin J Aeronaut* 2013;26(4):918–25.
11. Ran JH, Liu ZQ, Bai P. The effect of relative thickness to the dynamic aerodynamic characteristics about pitching airfoils. *Acta Aerodynamica Sin* 2008;26(2):178–85 Chinese.
12. Schroeder EJ, Baeder JD. Using computational fluid dynamics for micro-air vehicle airfoil validation and prediction. Reston: AIAA; 2005. Report No.: AIAA-2005-4841.
13. Langtry R, Menter F. Transition modeling for general CFD applications in aeronautics. Reston: AIAA; 2005. Report No.: AIAA-2005-0522.
14. Zhao YP, Ma DL, Qiao YH. Numerical simulation of low Reynolds number flows based on CFD. 2nd international conference on mechanics and mechatronics. Stafa-Zurich: Trans Tech Publications Ltd.; 2014.
15. Yan C. *Method and application of CFD*. 1st ed. Beijing: Beihang University Press; 2006, p. 224 Chinese.
16. McGranahan BD, Selig MS. Surface oil flow measurements on several airfoils at low Reynolds numbers. Reston: AIAA; 2003. Report No.: AIAA-2003-4067.

Ma Dongli received the Ph.D. degree in aircraft design from Beihang University in 1996. His main research interests are aircraft design and UAV technology.

Zhao Yanping received the M.S. degree in aircraft design from Beihang University in 2015. Her main research interest is aircraft design.

Qiao Yuhang received the B.S. degree from Beihang University in 2010. Now he is a Ph.D. candidate in the same university. His main research interest is aircraft design.

Li Guanxiang received the B.S. degree from Beihang University in 2013. Now he is a Ph.D. candidate in the same university. His main research interest is aircraft design.